ACS APPLIED MATERIALS & INTERFACES

Biological and Medical Applications of Materials and Interfaces

Delivery of temozolomide and N3-propargyl analog to brain tumors using an apoferritin nanocage

kaouthar Bouzinab, helen summers, Malcolm F.G. Stevens, Christopher J. Moody, Neil Rodney Thomas, Pavel Gershkovich, nicola weston, Marianne B. Ashford, Tracey D Bradshaw, and Lyudmila Turyanska

ACS Appl. Mater. Interfaces, **Just Accepted Manuscript** • DOI: 10.1021/acsami.0c01514 • Publication Date (Web): 19 Feb 2020

Delivery of temozolomide and N3-propargyl analog to brain tumors using an apoferritin nanocage

Kaouthar Bouzinab[a], Helen S. Summers[b], Malcolm F. G. Stevens[a], Christopher J. Moody[b], Neil R. Thomas[c], Pavel Gershkovich[a], Nicola Weston[d], Marianne B. Ashford[e], Tracey D. Bradshaw[a] and Lyudmila Turyanska[f*]*

[a]Biodiscovery Institute, School of Pharmacy, University of Nottingham, NG7 2RD, UK.

[b]School of Chemistry, University of Nottingham, NG7 2RD, UK.

[c]Biodiscovery Institute, School of Chemistry, University of Nottingham, NG7 2RD, UK.

[d]Nanoscale and Microscale Research Centre, University of Nottingham, NG7 2RD, UK.

[e]Advanced Drug Delivery, Pharmaceutical Sciences, R & D, AstraZeneca, Macclesfield, UK.

[f]Faculty of Engineering, University of Nottingham, NG7 2RD, UK

CORRESPONDING AUTHORS*:* *Tracey.Bradshaw@nottingham.ac.uk*

Lyudmila.Turyanska@nottingham.ac.uk

KEYWORDS: Temozolomide; Apoferritin; Glioblastoma multiforme; Drug delivery system.

This work was supported by the Engineering and Physical Sciences Research Council [grant number EP/L01646X/1; EP/L022494/1; EP/P03/1684/1] and the EPSRC Centre for Doctoral Training in Advanced Therapeutics and Nanomedicines

ABSTRACT

Glioblastoma multiforme (GBM) is a grade IV astrocytoma, which is the most aggressive form of brain tumor. The standard of care for this disease includes surgery, radiotherapy and temozolomide (TMZ) chemotherapy. Poor accumulation of TMZ at the tumor site, tumor resistance to drug and dose-limiting bone marrow toxicity eventually reduce the success of this treatment. Herein, we have encapsulated > 500 drug molecules of TMZ into the biocompatible protein nanocage, apoferritin (AFt), using a 'nanoreactor' method (AFt-TMZ). AFt is internalized by transferrin receptor 1-mediated endocytosis and is therefore able to facilitate cancer cell-uptake and enhance drug efficacy. Following encapsulation, the protein cage retained its morphological integrity and surface charge, hence its cellular recognition and uptake are not affected by the presence of this cargo. Additional benefits of AFt include maintenance of TMZ stability at pH 5.5 and drug release under acidic pH conditions, encountered in lysosomal compartments. MTT assays revealed that the encapsulated agents displayed significantly increased anti-tumor activity in U373V (vector control) and, remarkably the isogenic, U373M (MGMT expressing TMZ-resistant) GBM cell lines, with GI_{50} values < 1.5 μM for AFt-TMZ, compared to 35 μM and 376 μM for unencapsulated TMZ against U373V and U373M, respectively. The enhanced potency of AFt-TMZ was further substantiated by clonogenic assays. Potentiated G2/M cell cycle arrest following exposure of cells to AFt-TMZ indicated an enhanced DNA damage burden. Indeed, increased *O6*-methylguanine (*O6*-MeG) adducts in cells exposed to AFt-TMZ and subsequent generation of γH2AX foci, support the hypothesis that AFt significantly enhances the delivery of TMZ to cancer cells *in vitro*; overwhelming the direct *O6*-MeG repair conferred by MGMT. We have additionally encapsulated > 500 molecules of the N3-propargyl imidazotetrazine analog (N3P), developed to combat TMZ resistance, and demonstrated significantly enhanced activity of AFt-N3P against GBM and colorectal carcinoma cell lines. These studies support the use of AFt as

a promising nano-delivery system for targeted delivery, lysosomal drug release and enhanced imidazotetrazine potency for treatment of GBM and wider-spectrum malignancies.

1. INTRODUCTION

Glioblastoma multiforme (GBM), a grade (IV) astrocytoma, is the most prevalent and aggressive adult central nervous system (CNS) tumor; presenting heterogeneous, highly angiogenic, invasive and migratory characteristics.[1-4] GBM cells infiltrate healthy areas of the brain and are thus surrounded by a blood-brain tumor barrier and blood-brain barrier (BBB).[5] Surgical resection of the tumor followed by radiotherapy coupled with temozolomide (TMZ; **Figure 1a**) chemotherapy confers a median survival rate of ~ 15 months.[6] Despite the fact that TMZ is able to relatively easily cross the BBB by diffusion, there are concerns associated with poor accumulation of TMZ at the tumor site due to presence of active drug efflux transport proteins such as P-glycoprotein (Pgp) in the BBB and short TMZ plasma half-life ($t_{½}$).[7,8] Indeed, it has been estimated that < 1% of administered drug reaches the brain.[9] Furthermore, TMZ therapy harbors dose-limiting bone marrow toxicity, hence presenting an additional barrier to successful treatment.[10]

Intracellular drug resistance mechanisms further exacerbate efficacy. TMZ is a DNA methylating prodrug. Upon degradation, the active methyldiazonium cation is released and reacts with DNA purine bases, methylating *N3*-adenine, *O6*- and *N7*-guanine.[11] *O6*-methylguanine (*O6*-MeG) is the most cytotoxic product produced.[12,13] The mechanism of action of TMZ has been established[14-16] and it is now accepted that a deficiency in DNA mismatch repair (MMR) leading to *O6*-MeG-thymine mismatch tolerance and overexpression of *O6*-methylguanine-DNA methyltransferase (MGMT), which removes the methyl group from the *O6* position of guanine (restoring normal guanine), are major causes of TMZ resistance *in vitro* and clinically.[17,18] To overcome TMZ resistance, analogs of TMZ have been developed, whereby N3-methyl substitutions with for example N3-propargyl (N3P), have allowed analogs to evade recognition and removal by MGMT and exert activity independent of DNA mismatch repair (MMR) status.[19,20]

To enhance brain tumor drug accumulation for greater efficacy and to prevent dose-related toxicity, one approach has been to utilize drug delivery systems (DDS) for targeted drug delivery to tumors.[21-24] Apoferritin (AFt; 480 kDa) is a biocompatible protein cage with an external diameter of 12 nm and internal cavity of 8 nm.[25,26] The heavy (H) subunits of AFt bind to the transferrin receptor 1 (TfR1),[27,28] which is overexpressed in cancers (including gliomas) and is also abundantly present on the endothelium of the BBB.[29,30] Hence, AFt has been proposed as an active drug delivery system for therapeutic agents across the BBB *in vivo.*[31-33] Indeed, there remains an urgent need to develop effective DDS formulations for TMZ and its analogs to enhance efficacy, overcome drug resistance and improve prognoses for patients diagnosed with brain malignancies.

Herein, we report the encapsulation of TMZ into AFt for GBM-targeted drug delivery, *via* TfR1 uptake. AFt has 14 channels (~ 0.3 – 0.4 nm in diameter) that enable encapsulation of small molecules by diffusion (the so-called 'nanoreactor' route). *In vitro* studies have been carried out on the isogenic GBM cancer cell line pair, MGMT-low (U373V) and MGMT-transfected (U373M), together with MMR-deficient and Pgp overexpressing HCT116 colorectal carcinoma (CRC) cell lines and non-tumorigenic MRC-5 lung fibroblasts. Enhanced activity of drug within cancerous cells over non-transformed cells upon treatment with encapsulated versus naked drug was demonstrated. Supported by detection of enhanced *O6*-methylguanine (*O6*-MeG) adducts and γH2AX foci in GBM cells exposed to AFt-encapsulated (compared to naked) TMZ, we attribute the observed differential cytotoxicity to AFt-related enhanced delivery, uptake and intracellular retention by cancer cells, allowing release of (intact) TMZ in acidic lysosomes. We additionally demonstrate that further enhancement of activity can be achieved by AFt encapsulation of the TMZ analog bearing the N3P substitution. Our results offer a novel approach for imidazotetrazine formulations that address current limitations, such as drug stability and tumor resistance, associated with TMZ chemotherapy.

2. MATERIALS AND METHODS

AFt-drug encapsulation: Initially, the reductive demineralization of horse spleen ferritin (Ft; 92% L-subunit: 8% H-subunit) to AFt was carried out.[34] TMZ (Sigma-Aldrich) and N3P (synthesized by Helen S. Summers, University of Nottingham) were encapsulated into AFt by diffusion. For both nano-formulations, drug solution in DMSO (10 mM, 7.2 µmoles of TMZ; 6.3 µmoles of N3P) was added to AFt in 0.1 M sodium acetate (NaOAc) buffer (pH 5.5) solution (0.0045 mM, 0.009 µmoles) in small volume increments, every 30 mins (total time 4.5 h), under stirring at 4 °C. The formulations were ultra-filtered using an Amicon ultra-4 centrifugal filter (MWCO: 30 kDa) at 4000 x *g* for 4 mins and filtered through a 0.22 µm filter. Samples were stored at 4 °C for further studies.

Nanoparticle characterization: The hydrodynamic size and zeta potential of AFt and nano-formulations diluted in deionized water were measured using Malvern Zetasizer Nano ZS (backscatter angle 173°, λ = 633 nm, T = 25 °C). Samples were filtered (0.22 µm filter) prior to reading and measured in a disposable DTS1070 cell. Protein size was corroborated *via* red native-PAGE, whereby proteins were stained prior to electrophoresis with Ponceau S (Sigma-Aldrich) to impart negative charge whilst native structure was retained.[35] Using a native PAGE 4-16% Bis-Tris pre-cast gel (Invitrogen), samples (1 µg, 18 µL) alongside the NativeMark protein standard (Invitrogen, 5 µL) were resolved at 4 °C, for 1 h at 150 V followed by 1 h at 250 V. Gels were stained with Coomassie brilliant blue G250 for 1 h and left to de-stain overnight in water before imaging with Gene flow limited.

Assessment of encapsulation efficiency and drug loading: Drug concentration in solution was estimated from absorbance measurements using Varian Cary 50 UV-Vis spectrophotometer (λ = 330 nm for TMZ and λ = 328 nm for N3P) with a Suprasil quartz cuvette (Hellma Analytics) and the protein concentration was determined by Bradford assay (see Supplementary Materials, SI1).[36, 37] All measurements were performed in triplicate. For drug release studies, 400 µL of

AFt nano-formulations were added into a Slide-A-Lyzer 10 kDa MWCO device (Thermo Fisher Scientific) and samples were dialyzed at 37 °C and mixed at 150 rpm against 14 mL of either pH 5.5 NaOAc buffer (0.1 M) or pH 7.4 phosphate buffered saline (PBS). After 1, 3, 5, 7 and 24 h dialysis, drug concentration was measured by UV-Vis spectroscopy. Storage stability of AFt formulations at 4 °C, over 7 days, was also monitored for AFt and drug stability by using Malvern Zetasizer nano ZS, Bradford assay and UV-Vis spectrophotometer.

Cell culture studies: Human cell lines used include GBM, U373V (MGMT -) and U373M (MGMT +) (gifted by Schering Plough Corporation), colorectal carcinoma (CRC) HCT116 (MGMT +; hMLH1 -) and HCT116 VR (vincristine resistant; Pgp +)[38] and non-tumorigenic fetal lung fibroblast, MRC-5 (American Type Tissue Collection (ATCC)) cell lines. GBM cells were cultured in RPMI-1640 medium with 10% v/v fetal bovine serum (FBS), 1% v/v non-essential amino acids (NEAA), 50 μg/mL gentamicin and 400 μg/mL G418 (Corning). HCT116 cells were cultured in RPMI-1640 medium with 10% v/v FBS and MRC-5 cells were cultured in minimum essential medium (MEM) with 10% v/v FBS, 1% v/v NEAA, 1% v/v penicillin/streptomycin, 2 mM L-glutamine, 10 mM Hepes buffer and 0.075% v/v sodium bicarbonate. Cells were maintained in 5% CO_2 at 37 °C. All media and cell culture assay components except where otherwise specified were purchased from Sigma-Aldrich.

Growth inhibition of cells was monitored using the 3-(4,5-dimethylthiazol-2-yl)-2,5-diphenyltetrazolium bromide (MTT) assay. The MTT assay was performed in 96-well plates following 6-day test agent (naked drug, encapsulated drug and naked vehicle) exposure, and at the time of treatment at time zero (T0). Seeding densities for GBM cells were 650 cells/well and for HCT116 and MRC-5 cells, 400 cells/well. Test agent was introduced into wells (5 replicates per concentration) 24 h after cell-seeding. MTT reagent (400 μg/ml, Alfa Aesar) was added to each well and plates were incubated for 2 h at 37 °C. After 2 h, medium containing non-metabolized MTT was aspirated and the insoluble formazan product was dissolved in

DMSO (150 μL). Plates were placed on an orbital shaker for 5 mins and the absorbance was measured at λ = 570 nm with the Perkin Elmer Envision plate reader. At least 3 independent repeats for each test agent were performed.

For clonogenic assays, cells were seeded in 6-well plates (400 cells/well) and were exposed to TMZ, AFt-TMZ and AFt (50 μM TMZ; 0.057 μM AFt) for 24 h and 6 days. Thereafter, medium containing test agent was removed, cells were washed with PBS and fresh medium was introduced into wells. Plates were incubated at 37 °C and the assays terminated when colonies of ≥ 50 cells were observed in control wells. Colonies were washed with PBS, fixed with 100% methanol, stained with 0.05% methylene blue and counted. Duplicate repeats for each test agent were performed in at least 3 independent trials.

For live cell counts, GBM cells were seeded in 6-well plates at 1 x 10^4 cells/well and treated with TMZ, AFt-TMZ (TMZ: 50 μM; AFt: 0.057 μM) and AFt vehicle (0.057 μM) for 6 days. Then cells were collected by centrifugation (1200 rpm, 5 mins, 4 °C). Live cells were counted with a hemocytometer using trypan blue (Sigma-Aldrich).

Flow cytometry was carried out to examine cell cycle and for γH2AX foci analysis on GBM cells. For cell cycle analysis, cells were seeded in 6-well plates at 1 x 10^5 cells/well and treated with TMZ, AFt-TMZ (TMZ: 50 μM; AFt: 0.057 μM) and AFt (0.057 μM) for 72 h. Cells were collected and washed with PBS by centrifugation (1200 rpm, 5 mins, 4 °C). Cells were then incubated overnight at 4 °C, in the dark, with 500 μL of hypertonic fluorochrome solution (0.1% sodium citrate, 0.1% triton X-100, 50 μg/mL propidium iodide (PI) and 0.1 mg/mL ribonuclease A (RNase A) in deionized water). For γH2AX foci analysis, cells were seeded in 10 cm tissue culture treated Petri dish at 5 x 10^5 cells/dish and treated with TMZ, AFt-TMZ (TMZ: 50 μM; AFt: 0.057 μM and 100 μM; AFt: 0.1 μM) and AFt (0.057 and 0.1 μM) for 48 and 72 h. Cells were collected and stained using mouse anti-human phospho-histone H2A.X (Ser139) primary antibody (1° Ab), clone JBW301 (1:3333; Merck) and F(ab')2-goat anti-mouse IgG, IgM (H+L) Alexa-Fluor 488 secondary (2°) Ab (1:1750; Invitrogen). The fluorescence of 10000 mean gated events (single cells) was obtained using the Beckman Coulter FC500 flow cytometer. The data were processed using Weasel v3.0.2 software.

Indirect enzyme-linked immunosorbent assay (ELISA) was carried out for DNA *O6*-MeG quantification in GBM cells. Cells were seeded in 6-well plates at 0.1-1 x 10^5 cells/well and treated with TMZ and AFt-TMZ (50 μM) for 4, 24, 72 and 144 h. The purification of DNA from cells was carried out using the QIAGEN Blood & Cell Culture DNA mini purification kits, following the manufacturer's procedure. Double-stranded DNA (1 μg) was then digested with the Timesaver MspI restriction enzyme kit (New England Biolabs), following the manufacturer's procedure, and made single-stranded by heating at 95 °C for 10 mins before rapidly transferring to ice for at least 15 mins. ELISA was then performed using the IgG (Total) Mouse Uncoated ELISA kit (Invitrogen), following the manufacturer's procedure with some modifications. Briefly, a 96-well plate was pre-coated with 1% w/v protamine sulfate (Sigma-Aldrich) at RT for 1 h, removed and washed 5 times with a jet of milli-Q water. Wells were then coated with DNA (10 ug/mL; 100 μL) diluted in coating buffer 1x and incubated overnight on a shaker at RT. Wells were washed (3x) with eBioscience wash buffer 1x (Invitrogen) and blocked with blocking buffer 2x for 2 h, at room temperature (RT). Samples were incubated with the 1° monoclonal Ab, mouse anti-human *O6*-MeG (0.2 μg/mL; Axxora) for 1.5 h at RT, followed by incubation with 2° HRP-conjugated anti-mouse IgG polyclonal Ab (1:250) for 1 h at RT. Wells were then treated with the tetramethylbenzidine (TMB) substrate solution (100 μL) for 15 mins at RT in the dark, quenched with stop solution (100 μL; Invitrogen) for 5 mins at RT and absorbance read at λ = 450 nm on a Perkin Elmer Envision plate reader. At least 3 independent repeats for each test agent were performed.

Western blot: For protein extraction, cells were collected by centrifugation (1200 rpm, 5 mins, 4 °C) and lysed in Nonidet-P40 lysis buffer. Protein concentrations were determined by

Bradford assay.[36,37] Protein fractions (50 µg) were separated by SDS-PAGE (10% resolving gel), transferred onto a nitrocellulose membrane (GE Healthcare Life Sciences) using the Trans-Blot Turbo Transfer System (Bio-Rad) and blocked in 5% skimmed milk in TBST (tris-buffered saline, Tween 20) for 1 h. Membranes were incubated at 4 °C overnight with the following monoclonal 1° Abs, rabbit anti-human TfR1 (1:1000), MGMT (1:1000), glyceraldehyde 3-phosphate dehydrogenase (GAPDH; loading control; 1:1000) (all from Cell Signaling Technology), mouse anti-human Scavenger Receptor Class A Member 5 (SCARA5; 1:1000) and transferrin receptor 2 (TfR2; 1:250) (both from R&D systems a bio-techne brand). Membranes were then incubated with 2° Ab (1:4000) for 1 h at RT using either goat anti-rabbit or goat anti-mouse polyclonal antibodies conjugated with horseradish peroxidase (Dako). Bands were visualized on a C-DiGit blot scanner (LI-COR Biosciences) after incubating the membranes with ECL reagent (GE Healthcare) for 5 mins.

Imaging cellular morphology: For environmental scanning electron microscopy (ESEM), a TGS1x0.2 Gold Slot grid (EM Resolutions) was placed at the bottom of a 6-well plate and cells were seeded at 1 x 10^5 cells/well. After 24 h exposure to TMZ and AFt-TMZ (50 µM), cells were fixed with 3.7% v/v formaldehyde in PBS for 5 mins. The grids were washed and stored in PBS. Immediately prior to imaging, grids were rinsed with deionized water and mounted on a stage set at 3 °C. The chamber pressure was dropped to 5.15 Torr, with humidity set to 87 %. Images were acquired using FEI Quanta 650 ESEM operating using a 5 kV electron beam and magnification x1000. For confocal microscopy, GBM cells were seeded in an 8-well µ-slide plate (Ibidi) at 1 x 10^4 cells/well and treated for 24 h with TMZ and AFt-TMZ (50 µM). Following treatment, cells were washed with PBS, fixed with 3.7% v/v formaldehyde (15 mins) and permeabilized with 0.1% v/v triton X-100. Cells were then co-stained for 1 h with F-actin phalloidin-iFluor 633 (1x) and nuclear DAPI (0.02 µg/ml) stains. Wells were washed twice with PBS before storing in PBS (200 µL) for imaging. Imaging was performed with a 63x water magnification lens using Zeiss Elyra PS1 super resolution microscope with DAPI excitation at 405 nm and phalloidin excitation at 633 nm. Confocal images were analyzed using the Fiji Image J software.

Statistical analysis. Two-way or three-way ANOVA analysis function on GraphPad Prism version 8.2.1 was used to determine the differences between multiple groups ($n \geq 3$). Values of $^{*}P$ or $^{\#}P < 0.05$, $^{**}P$ or $^{\#\#}P < 0.01$, $^{***}P$ or $^{\#\#\#}P < 0.001$ and $^{****}P$ or $^{\#\#\#\#}P < 0.0001$ were considered as statistically significant. Data are represented as the means ± SD.

3. RESULTS AND DISCUSSION

The AFt protein cage has an external diameter ~ 12 nm suitable for passive targeting *via* the enhanced permeability and retention (EPR) effect.[39] TfR1 binding sites on the H-polypeptide subunits of AFt allow active targeting of AFt-encapsulated cargo. TfR1 has been shown to be overexpressed by GBM (but not glial) and present on BBB endothelial cells, but not peripheral endothelium.[30] TfR1 has been shown to be an important receptor for cancers due to their increased iron demand.[40] We hence evaluated the loading of TMZ into AFt for GBM targeting, with the goal to achieve enhanced transport of the molecules across the BBB, delivery to, and accumulation within cancer cells. AFt-encapsulation of TMZ may also minimize premature degradation and elimination, efflux (mediated by Pgp) and drug-related side effects. The small size of the test agent (< 300 g/mol) allows its encapsulation *via* the 'nanoreactor' route, where passive diffusion across the 0.3 - 0.4 nm channels is feasible.[37,41,42] Briefly, test agent was added gradually over 4.5 h to AFt at pH 5.5 to permit encapsulation under diffusion to take place (**Figure 1b**) and to avoid TMZ degradation, which occurs at physiological pH ~ 7.4 (*in vitro* $t_{½}$ of TMZ at pH 7.4 is 1.9 h;[8] at pH 5.5 $t_{½} > 100$ h). We achieved 84.3 ± 5.2% encapsulation efficiency (EE) and 18.7 ± 2.3% drug loading (DL), which corresponds to ~ 520 drug molecules per AFt cage (see also Supplementary Information, SI1). The integrity of the AFt cage following drug encapsulation and absence of drug attachment to the AFt exterior was confirmed by DLS and zeta potential measurements; no noticeable change in either hydrodynamic size or zeta potential was observed, with average hydrodynamic diameter of 13.3 ± 0.9 nm and zeta potential of -12.7 ± 0.3 mV for AFt before and after TMZ encapsulation (**Figure 1c**). Native PAGE of AFt-TMZ revealed protein bands at molecular weight (MW) ~ 480 and 720 kDa (dimer), comparable to those of AFt alone (**Figure 1d**), confirming successful encapsulation of the agents inside the AFt cavity. By optimizing the encapsulation conditions and performing step-wise addition of the drug, we achieved improved drug loading (~ 520 molecules per AFt cage) compared to previously reported values of up to 100 – 350 molecules of GW608 and its derivatives and 185 molecules of triazene, 5-(3-methyltriazen-1-yl) imidazole-4-carboxamide (MTIC).[37,43] We attribute enhanced DL, to the small molecular weight and good solubility profiles of TMZ.

We assessed the release of drugs from AFt under physiologically relevant conditions (T = 37 °C, pH 7.4 and pH 5.5; see Supplementary Information SI1, Figure S2) and observed slower drug release within the first 3 h at pH 7.4 compared to pH 5.5. This observation is consistent with the expectation that AFt channels are narrower at more alkali pH and gradually widen as the capsule relaxes with increasing acidity.[44] The storage stability of the AFt formulation (at T = 4 °C) was monitored and no apparent change in protein size, zeta potential or drug:AFt ratio were observed over a period of at least 7 days (Supplementary Information SI1, Figure S3).

The *in vitro* anti-cancer activity of TMZ delivered by AFt was subsequently evaluated. Initially, MTT assays were employed and the following cell lines utilized for our studies: U373V (MGMT -), U373M (MGMT +) GBM; HCT116 (MMR deficient), HCT116 VR (Pgp +) CRC and non-cancerous MRC-5 fibroblasts. The growth inhibitory activity of AFt-TMZ was compared to unencapsulated (naked) TMZ. The cells were exposed to test agent with concentrations ranging from 0.001 - 1000 µM. Cellular growth inhibition (estimated GI_{50} values) was determined (**Figure 2**). Cells were exposed to test agents for 6 days, allowing enough time for a minimum of 2 cell cycle rounds, DNA methylation and MMR activation. AFt-TMZ demonstrated markedly enhanced activity over naked TMZ. GI_{50} values of 35 µM and 376 µM were calculated for TMZ in U373V and U373M cells respectively. Remarkably, AFt-TMZ demonstrated significantly lower GI_{50} values (enhanced activity) of < 1.5 µM in both U373V and U373M cell lines. Of interest, and contrary to expectations, AFt-encapsulated TMZ displayed enhanced activity over naked TMZ in cell lines that showed resistance to TMZ, where resistance was conferred by MGMT (532-fold enhanced activity in U373M), MMR loss (22-fold in HCT116) and additionally Pgp expression (24-fold in HCT116 VR).

Cancer-selective activity was also seen, with AFt-TMZ demonstrating enhanced activity against cancer cells over fibroblasts by ~ 5-fold. Alone, AFt did not display growth inhibitory activity against any of the cell lines at concentrations ≤ 1 µM (equivalent to the highest concentration of AFt in AFt-drug used in the assay). In support of this study, live cell count assays (Supplementary Information, SI2) demonstrated greater significant loss of viable cells with AFt-TMZ treatment against U373M compared to naked TMZ ($P < 0.0001$). Interestingly, Fang *et al*. demonstrated that conjugation of TMZ to chitosan nanoparticles could partially overcome TMZ-resistance.[23] Kumari *et al*. also reported this phenomenon with TMZ-loaded lactoferrin nanoparticles.[24] Recently reported is the AFt-encapsulation of the combined TMZ-intermediate, MTIC, with copper.[43] We postulate that the enhanced activity of TMZ encapsulated within AFt is due to a different mode of cellular uptake (*via* TfR1 recognition). AFt rapidly enters and accumulates inside lysosomes following TfR1 receptor mediated endocytosis,[27] therefore evasion of Pgp efflux may be possible. Consequently, enhanced intracellular accumulation of TMZ results in greater potency.

In order to test this hypothesis, we examined cellular expression of proteins responsible for AFt uptake and resistance to TMZ. Protein lysates prepared from the cancer cells used in this study revealed TfR1 expression whereas in MRC-5 lysates, expression was below the limit of detection (**Figure 3** and supplementary Figure S5). Since the expression of SCARA5 and TfR2 was not observed, we conclude that TfR1 is the receptor responsible for AFt uptake, providing some selective anti-cancer activity for our formulation. Western blot also confirmed the presence of MGMT, which confers TMZ resistance, in U373M and its absence in U373V.

To substantiate the results of AFt-TMZ activity against TMZ-resistant U373M, clonogenic assays were employed. **Figure 4** illustrates the survival fraction of U373V and U373M colonies after 24 h and 6 days exposure to naked and encapsulated TMZ (see also Supplementary Information SI2). AFt alone had negligible effect on colony numbers confirming the biocompatibility of this drug delivery vehicle, however, AFt-encapsulation of TMZ augmented the drug`s inhibition of colony formation in both U373V and U373M GBM cells. TMZ alone (50 µM) potently inhibited U373V colony formation by 68% and 84% after 24 h and 6 d exposure, respectively; whereas, U373M cells demonstrated much greater resistance to naked TMZ challenge (colony formation inhibited by 14% and by 35% after 24 h and 6 d exposure, respectively). In contrast, 24 h and 6 d AFt-TMZ exposure potently inhibited U373M colony formation by 47% and 76% respectively. U373M cells were significantly less able to survive AFt-TMZ challenge (compared to naked TMZ) and form progeny colonies; AFt-TMZ displayed 2.7-fold enhanced toxicity compared to naked TMZ, supporting MTT assays and cell counts further demonstrating that AFt-delivery of TMZ is able to weaken tumor resistance to TMZ mediated by MGMT.

Following the assessment of AFt-TMZ cytotoxicity, GBM cell cycle progression was probed after 72 h exposure of cells to TMZ and AFt-TMZ. Treatment periods of 72 h were adopted to allow cells to complete at least one division for detection of putative cell cycle perturbation by AFt-TMZ. It is known that TMZ (in the absence of MGMT) alkylates DNA causing S and G2/M arrest.[13,14] G2/M arrest can be seen following treatment with TMZ in U373V cells only; however, both U373V and U373M cells expressed greater G2/M- and S-phase arrest following exposure to AFt-TMZ (**Figure 5a**, and Supplementary Information, SI2). Compared to U373V control populations, S-phase arrest was increased by ~ 2.5- and 2.6-fold with TMZ and AFt-TMZ, respectively; G2/M-phase arrest was increased by ~ 2.3- and 2.8-fold, respectively. As for U373M, S- and G2/M-phase arrest was increased by 1.87- and 2-fold, respectively, following treatment with AFt-TMZ. TMZ alone failed to significantly perturb U373M cell cycle progression. Cell cycle profiles indistinguishable from controls were observed following exposure of cells to AFt alone. Assessment of *O6*-MeG levels in the DNA of cells following treatment with TMZ and AFt-TMZ (4 – 144 h), revealed that AFt-TMZ delivered significantly more ($P < 0.001$) methyl groups to *O6*-guanine then TMZ alone (**Figure 5b**).

Since AFt-TMZ was shown to transcend the resistance systems in GBM cells, evoking significantly enhanced activity over TMZ alone, we sought to establish whether the increased *O6*-MeG levels and S- and G2/M-phase arrest translated to greater DNA damage following treatment for 48 and 72 h. The presence of γH2AX foci is indicative of DNA double strand breaks and as such, our studies have demonstrated that greater levels of γH2AX foci were observed following treatment of U373V and U373M cells with AFt-TMZ (compared to TMZ alone; **Figure 5c**). These levels were shown to increase in both a time- and concentration-dependent manner. In U373V and U373M, 72 h exposure to 50 μM AFt-TMZ yielded respectively 1.2- and 1.4-fold significantly more DNA double strand breaks over TMZ alone ($P < 0.001$). This corroborated well with the trends observed in cell cycle and *O6*-MeG analyses.

We further evaluated the effect of AFt-TMZ treatment on GBM cells using ESEM in order to observe changes to the cell surface after brief exposure of cells to test agents. It was apparent that the spread of the cells was greatly affected by AFt-TMZ, more so than by naked TMZ after 24 h treatment exposure (**Figure 6**). In contrast to the control cells, those treated with AFt-TMZ appeared more shrunken, with blebs apparent on their surfaces; being most obvious on U373M. Confocal microscopy studies carried out on stained actin filaments using phalloidin further corroborated the ESEM work. The intensity of the phalloidin stain was at its lowest with AFt-TMZ; a more shrunken cellular morphology most likely indicates reduced uptake of F-actin stain (Supplementary Information, SI2, Figure S9). Cell shrinkage and blebbing may signify apoptosis. F-actin cytoskeleton is an essential component in regulation of cell shape, migration and division and its reduction infers loss of these capabilities.[45] These methodologies have demonstrated that AFt-TMZ affects cellular morphology as early as 24 h post treatment.

The promising, enhanced anti-cancer activity achieved with AFt-TMZ encouraged us to pursue AFt-encapsulation of N3P, an analog of TMZ where N3-methyl has been replaced with a propargyl moiety (**Figure 7**). N3P was designed to deliver propargyl lesions onto susceptible DNA bases that cannot be removed by MGMT. Indeed, TAQ polymerase assays demonstrated alkylation at runs of guanine – akin to those caused by TMZ, and anti-tumor activity was seen irrespective of MGMT or MMR status.[19,20] However, N3P possesses inferior (in comparison to TMZ) pharmacokinetic properties ($t_{½}$ = 49 min at pH 7.4), potentially thwarting efficient delivery to the brain and therapeutic utility. Like TMZ, N3P is acid-stable ($t_{½}$ > 100 h at pH 5.5), therefore, N3P was encapsulated within AFt cages using the same diffusion method optimized for TMZ. Similar loading efficiency of ~ 525 molecules per AFt capsule was achieved (EE = 70.5 ± 3.3% and DL = 20.5 ± 3.1%). No noticeable change in hydrodynamic size and zeta potential was observed, with average hydrodynamic diameter of

13.1 ± 0.7 nm and zeta potential of -12.5 ± 0.4 mV for AFt before and after N3P encapsulation (**Figure 7a**). Native PAGE of AFt-N3P revealed protein bands at MW ~ 480 and 720 kDa, comparable to those of AFt alone; confirming successful encapsulation of the agent inside the AFt cavity. *In vitro* growth inhibitory studies on GBM cell lines, U373V (MGMT –) and U373M (MGMT +), HCT 116 (MMR deficient) and non-cancerous MRC-5 fibroblasts (**Figure 7b**) demonstrated enhanced activity with lower GI_{50} values compared to TMZ in both GBM cell lines: GI_{50} value of < 0.25 μM for AFt-N3P. The AFt-N3P formulation retained a degree of selectivity, with ~ 9-fold greater activity in cancer cells compared to fibroblasts.

Therefore, development of AFt-formulations of TMZ and N3P represents a promising strategy to challenge TMZ resistance in malignant brain tumors such as GBM, and wider spectrum cancer phenotypes. Furthermore, the surface of AFt can be modified with additional surface ligands (e.g. GKRK peptides) for enhanced tumor accumulation *in vivo* and BBB penetrance.[31,46] Preclinical effects of AFt delivery of imidazotetrazine molecules will be further evaluated *in vivo*.

4. CONCLUSIONS

In conclusion, we have successfully loaded > 500 molecules of TMZ and N3P per AFt cage, *via* the nanoreactor route, achieving EE > 70% and DL > 18%, and maintaining AFt capsule integrity. *In vitro* studies demonstrated that both AFt nano-formulations displayed significantly enhanced activity over naked drugs against MGMT +/- GBM cell lines. Most intriguingly, this includes AFt-TMZ, which *in vitro* overcame tumor resistance mediated by MGMT. Accumulation of *O6*-MeG adducts, cell cycle arrest and subsequent generation of γH2AX in U373M support the hypothesis that TfR1, expressed by cancer cell lines used in this study, mediates increased intracellular accumulation of TMZ that is able to overwhelm the suicide repair protein MGMT and confer sensitivity to TMZ in MGMT + GBM cells. If *O6*-guanine methylation outpaces MGMT protein synthesis, its depletion would ensue [47] – as is indicated following exposure of U373M cells to AFt-TMZ (Bouzinab unpublished results). Moreover, evidence suggests other mechanisms conferring tolerance or resistance to TMZ may be weakened (including MMR-deficiency and Pgp expression) following its encapsulation in AFt. In addition, AFt encapsulation of imidazotetrazine analog N3P resulted in enhanced anti-tumor activity and cancer cell line-selectivity. Importantly, AFt alone was non-toxic. These findings lay the foundations for AFt, a biocompatible, species-specific nanosized biomaterial with built in targeting, to deliver concentrated amounts of anti-cancer small molecules to tumors.

ASSOCIATED CONTENT

Supporting Information. Supporting information included methodology and characterization data. The following file is available: Supporting Information.pdf

AUTHOR INFORMATION

Corresponding Authors

* Dr Lyudmila Turyanska Lyudmila.Turyanska@nottingham.ac.uk

Dr Tracey D Bradshaw Tracey.Bradshaw@nottingham.ac.uk

University of Nottingham, NG7 2RD Nottingham, UK

Author Contributions

The manuscript was written through contributions of all authors. All authors have given approval to the final version of the manuscript.

Funding Sources

Engineering and Physical Sciences Research Council [grant number EP/L01646X/1 and EP/L022494/1].

CONFLICTS OF INTEREST

The authors declare no conflicts of interest and no competing financial interest.

ACKNOWLEDGMENTS

This work was funded by the Engineering and Physical Sciences Research Council [grant number EP/L01646X/1; EP/L022494/1; EP/P03/1684/1] and the EPSRC Centre for Doctoral Training in Advanced Therapeutics and Nanomedicines; University of Nottingham and AstraZeneca. The authors acknowledge the Nanoscale and Microscale Research Centre (nmRC) for providing access to instrumentation and to Dr. David Onions and Dr. Robert Markus for useful discussions and technical support. Authors acknowledge support from Children with Cancer UK and Josephine R. Poole for cover art.

REFERENCES

(1) Parsons, D.; Jones, S.; Zhang, X.; Lin, J.; Leary, R.; Angenendt, P.; Mankoo, P.; Carter, H.; Siu, I. M.; Gallia, G. L.; Olivi, A.; McLendon, R.; Rasheed, B. A.; Keir, S.; Nikolskaya, T.; Nikolsky, Y.; Busam, D. A.; Tekleab, H.; Diaz, L. A., Jr.; Hartigan, J.; Smith, D. R.; Strausberg, R. L.; Marie, S. K.; Shinjo, S. M.; Yan, H.; Riggins, G. J.; Bigner, D. D.; Karchin, R.; Papadopoulos, N.; Parmigiani, G.; Vogelstein, B.; Velculescu, V. E.; Kinzler, K. W. An Integrated Genomic Analysis of Human Glioblastoma Multiforme. *Science* **2008**, *321*, 1807-1812.

(2) Phillips, H. S.; Kharbanda, S.; Chen, R.; Forrest, W. F.; Soriano, R. H.; Wu, T. D.; Misra, A.; Nigro, J. M.; Colman, H.; Soroceanu, L.; Williams, P. M.; Modrusan, Z.; Feuerstein, B. G.; Aldape, K. Molecular subclasses of high-grade glioma predict prognosis, delineate a pattern of disease progression, and resemble stages in neurogenesis. *Cancer Cell* **2006**, *9*, 157-173.

(3) Beroukhim, R.; Getz, G.; Nghiemphu, L.; Barretina, J.; Hsueh, T.; Linhart, D.; Vivanco, I.; Lee, J. C.; Huang, J. H.; Alexander, S.; Du, J.; Kau, T.; Thomas, R. K.; Shah, K.; Soto, H.; Perner, S.; Prensner, J.; Debiasi, R. M.; Demichelis, F.; Hatton, C.; Rubin, M. A.; Garraway, L. A.; Nelson, S. F.; Liau, L.; Mischel, P. S.; Cloughesy, T. F.; Meyerson, M.; Golub, T. A.; Lander, E. S.; Mellinghoff, I. K.; Sellers, W. R. Assessing the significance of chromosomal aberrations in cancer: Methodology and application to glioma. *Proc. Natl. Acad. Sci. U.S.A.* **2007**, *104*, 20007-20012.

(4) Smith, C. L.; Kilic, O.; Schiapparelli, P.; Guerrero-Cazares, H.; Kim, D. H.; Sedora-Roman, N. I.; Gupta, S.; O'Donnell, T.; Chaichana, K. L.; Rodriguez, F. J.; Abbadi, S.; Park, J.; Quiñones-Hinojosa, A.; Levchenko, A. Migration Phenotype of Brain-Cancer Cells Predicts Patient Outcomes. *Cell Rep.* **2016**, *15*, 2616-2624.

(5) Watkins, S.; Robel, S.; Kimbrough, I. F.; Robert, S. M.; Ellis-Davies, G.; Sontheimer, H. Disruption of astrocyte–vascular coupling and the blood–brain barrier by invading glioma cells. *Nat. Commun.* **2014**, *5*, 4196.

(6) Brodbelt, A.; Greenberg, D.; Winters, T.; Williams, M.; Vernon, S.; Collins, V. P. Glioblastoma in England: 2007–2011. *Eur. J. Cancer* **2015**, *51*, 533-542.

(7) de Gooijer, M. C.; de Vries, N. A.; Buckle, T.; Buil, L. C. M.; Beijnen, J. H.; Boogerd, W.; van Tellingen, O. Improved Brain Penetration and Antitumor Efficacy of Temozolomide by Inhibition of ABCB1 and ABCG2. *Neoplasia* **2018**, *20*, 710-720.

(8) Baker, S. D.; Wirth, M.; Statkevich, P.; Reidenberg, P.; Alton, K.; Sartorius, S. E.; Dugan, M.; Cutler, D.; Batra, V.; Grochow, L. B.; Donehower, R. C.; Rowinsky, E. K. Absorption, metabolism, and excretion of 14C-temozolomide following oral administration to patients with advanced cancer. *Clin. Cancer Res.* **1999**, *5*, 309-17.

(9) Groothuis, D. R. The blood-brain and blood-tumor barriers: A review of strategies for increasing drug delivery. *Neuro-Oncology* **2000**, *2*, 45-59.

(10) Newton, S.; Kalamaha, K.; Fernandes, H. Temozolomide-induced Aplastic Anemia Treated with Eltrombopag and Granulocyte Colony Stimulating Factor: A Report of a Rare Complication. *Cureus* **2018**, *10*, e3329.

(11) Zhang, J.; Stevens, M. F.; Bradshaw, T. D. Temozolomide: Mechanisms of Action, Repair and Resistance. *Curr. Mol. Pharmacol.* **2012**, *5*, 102-114.

(12) Denny, B. J.; Wheelhouse, R. T.; Stevens, M. F.; Tsang, L. L. Slack, J. A. NMR and Molecular Modeling Investigation of the Mechanism of Activation of the Antitumor Drug Temozolomide and Its Interaction with DNA. *Biochemistry* **1994**, *33*, 9045-9051.

(13) Tisdale M. J. Antitumour imidazotetrazines—XV: Role of guanine O^6 alkylation in the mechanism of cytotoxicity of imidazotetrazinones. *Biochem. Pharmacol.* **1987**, *36*, 457-462.

(14) Mojas, N.; Lopes, M.; Jiricny, J. Mismatch repair-dependent processing of methylation damage gives rise to persistent single-stranded gaps in newly replicated DNA. *Genes Dev.* **2007**, *21*, 3342-3355.

(15) He, Y.; Kaina, B. Are There Thresholds in Glioblastoma Cell Death Responses Triggered by Temozolomide? *Int. J. Mol. Sci.* **2019**, *20*, 1562.

(16) Roos, W.; Baumgartner, M.; Kaina, B. Apoptosis triggered by DNA damage O6-methylguanine in human lymphocytes requires DNA replication and is mediated by p53 and Fas/CD95/Apo-1. *Oncogene* **2004**, *23*, 359-367.

(17) Cejka, P.; Stojic, L.; Mojas, N.; Russell, A. M.; Heinimann, K.; Cannavó, E.; di Pietro, M.; Marra, G.; Jiricny, J. Methylation-induced G2/M arrest requires a full complement of the mismatch repair protein hMLH1. *EMBO J.* **2003**, *22*, 2245-2254.

(18) Kitange, G. J.; Carlson, B. L.; Schroeder, M. A.; Grogan, P. T.; Lamont, J. D.; Decker. P. A.; Wu, W.; James, C. D.; Sarkaria, J. N. Induction of MGMT expression is associated with temozolomide resistance in glioblastoma xenografts. *Neuro-Oncology* **2009**, *11*, 281-291.

(19) Zhang, J.; Hummersone, M. G.; Matthews, C. S.; Stevens, M. F. Bradshaw, T. D. N3-Substituted Temozolomide Analogs Overcome Methylguanine-DNA Methyltransferase and Mismatch Repair Precipitating Apoptotic and Autophagic Cancer Cell Death. *Oncology* **2015**, *88*, 28-48.

(20) Cousin, D.; Zhang, J.; Hummersone, M. G.; Matthews, C. S.; Frigerio, M.; Bradshaw, T. D.; Stevens, M. F. Antitumor imidazo[5,1-d]-1,2,3,5-tetrazines: compounds modified at the 3-position overcome resistance in human glioblastoma cell lines. *Med. Chem. Commun.* **2016**, *7*, 2332-2343.

(21) Kim, J.; Ahn, S. I.; Kim, Y. Nanotherapeutics engineered to cross the blood-brain barrier for advanced drug delivery to the central nervous system. *J. Ind. Eng. Chem.* **2019**, *73*, 8-18.

(22) Oberoi, R. K.; Parrish, K. E.; Sio, T. T.; Mittapalli, R. K.; Elmquist, W. F.; Sarkaria, J. N. Strategies to improve delivery of anticancer drugs across the blood–brain barrier to treat glioblastoma. *Neuro-Oncology* **2015**, *18*, 27-36.

(23) Fang, C.; Wang, K.; Stephen, Z. R.; Mu, Q.; Kievit, F. M.; Chiu, D. T.; Press, O. W.; Zhang, M. Temozolomide Nanoparticles for Targeted Glioblastoma Therapy. *ACS Appl. Mater. Interfaces* **2015**, *7*, 6674-6682.

(24) Kumari, S.; Ahsan, S. M.; Kumar, J. M.; Kondapi, A. K.; Rao, N. M. Overcoming blood brain barrier with a dual purpose Temozolomide loaded Lactoferrin nanoparticles for combating glioma (SERP-17-12433). *Sci. Rep.* **2017**, *7*, 6602.

(25) Ford, G. C.; Harrison, P. M.; Rice, D. W.; Smith, J. M.; Treffry, A.; White, J. L.; Yariv, J. Ferritin: Design and Formation of an Iron-Storage Molecule. *Philos. Trans. R. Soc., B* **1984**, *304*, 551-565.

(26) Crichton. R. R.; Bryce, C. F. Subunit interactions in horse spleen apoferritin. Dissociation by extremes of pH. *Biochem. J.* **1973**, *133*, 289-299.

(27) Li, L.; Fang, C. J.; Ryan, J. C.; Niemi, E. C.; Lebrón, J. A.; Björkman, P. J.; Arase, H.; Torti, F. M.; Torti, S. V.; Nakamura, M. C.; Seaman, W. E. Binding and uptake of H-ferritin are mediated by human transferrin receptor-1. *Proc. Natl. Acad. Sci. U.S.A.* **2010**, *107*, 3505-3510.

(28) Zhang, L.; Li, L.; Di Penta, A.; Carmona, U.; Yang, F.; Schöps, R.; Brandsch, M.; Zugaza, J. L.; Knez, M. H-Chain Ferritin: A Natural Nuclei Targeting and Bioactive Delivery Nanovector. *Adv. Healthcare Mater.* 2015, *4*, 1305–1310.

(29) Jefferies, W. A.; Brandon, M. R.; Hunt, S. V.; Williams, A. F.; Gatter, K. C.; Mason, D. Y. Transferrin receptor on endothelium of brain capillaries. *Nature* **1984**, *312*, 162-163.

(30) Johnsen, K. B.; Burkhart, A.; Melander, F.; Kempen, P. J.; Vejlebo, J. B.; Siupka, P.; Nielsen, M. S.; Andresen, T. L.; Moos, T. Targeting transferrin receptors at the blood-brain barrier improves the uptake of immunoliposomes and subsequent cargo transport into the brain parenchyma. *Sci. Rep.* **2017**, *7*, 10396.

(31) Zhai, M, Wang, Y.; Zhang, L.; Liang, M.; Fu, S.; Cui, L.; Yang, M.; Gong, W.; Li, Z.; Yu, L.; Xie, X.; Yang, C.; Yang, Y.; Gao, C. Glioma targeting peptide modified apoferritin nanocage. *Drug Delivery* **2018**, *25*, 1013-1024.

(32) Chiou, B.; Connor, J. R. Emerging and dynamic biomedical uses of ferritin. *Pharmaceuticals* **2018**, *11*, E124.

(33) Macone, A.; Masciarelli, S.; Palombarini, F.; Quaglio, D.; Boffi, A.; Trabuco, M. C.; Baocco, P.; Fazi, F.; Bonamore, A. Ferritin nanovehicle for targeted delivery of cytochrome C to cancer cells. *Sci. Rep.* **2019**, *9*, 11749.

(34) Wong, K. K.; Cölfen, H.; Whilton, N. T.; Douglas, T.; Mann, S. Synthesis and characterization of hydrophobic ferritin proteins. *J. Inorg. Biochem.* **1999**, *76*, 187-195.

(35) Dráb, T.; Kračmerová, J.; Tichá, I.; Hanzlíková, E.; Tichá, M.; Ryšlavá, H.; Doubnerová, V.; Maňásková-Postlerová, P.; Liberda, J. Native Red Electrophoresis – A new method suitable for separation of native proteins. *Electrophoresis* **2011**, *32*, 3597-3599.

(36) Bradford, M. M. A rapid and sensitive method for the quantitation of microgram quantities of protein utilizing the principle of protein-dye binding. *Anal. Biochem.* **1976**, *72*, 248-254.

(37) Breen, A. F.; Wells, G.; Turyanska, L.; Bradshaw, T. D. Development of novel apoferritin formulations for antitumour benzothiazoles. *Cancer Reports* **2019**, *2*, e1155.

(38) Qazzaz, M. E.; Raja, V. J.; Lim, K. H.; Kam, T. S.; Lee, J. B.; Gershkovich, P.; Bradshaw, T. D. *In vitro* anticancer properties and biological evaluation of novel natural alkaloid jerantinine b. *Cancer Lett.* **2016**, *370*, 185-197.

(39) Grobmyer, S. R.; Moudgil, B. M. In Cancer nanotechnology: methods and protocols; Methods in molecular biology (Clifton, N.J.), Vol. 624; Springer protocols; Humana Press: New York, 2010.

(40) Torti, S. V.; Torti, F. M. Iron and cancer: more ore to be mined. *Nat. Rev. Cancer* **2013**, *13*, 342-355.

(41) Bouzinab, K.; Summers, H.; Zhang, J.; Stevens, M. F. G.; Moody, C. J.; Turyanska, L.; Thomas, N. R.; Gershkovich, P.; Ashford, M. B.; Vitterso, E.; Storer, L. C D.; Grundy, R.; Bradshaw, T. D. In search of effective therapies to overcome resistance to temozolomide in brain tumours. *Cancer Drug Resist.* **2019**, *2*, 1018-1031.

(42) Kuruppu, A. I.; Zhang, L.; Collins, H.; Turyanska, L.; Thomas, N. R.; Bradshaw, T. D. An apoferritin-based drug delivery system for the Tyrosine Kinase Inhibitor Gefitinib. *Adv. Healthcare Mater.* **2015**, *4*, 2816-2821.

(43) Li, X.; Shao, F.; Sun, J.; Du, K.; Sun, Y.; Feng, F. Enhanced copper−temozolomide interactions by protein for chemotherapy against glioblastoma multiforme. *ACS Appl. Mater. Interfaces* **2019**, *11*, 41935-41945.

(44) Kim, M.; Rho, Y.; Jin, K. S.; Ahn, B.; Jung, S.; Kim, H.; Ree, M. pH-Dependent Structures of Ferritin and Apoferritin in Solution: disassembly and reassembly. *Biomacromolecules* **2011**, *12*, 1629-1640.

(45) Stricker, J.; Falzone, T.; Gardel, M. Mechanics of the F-actin Cytoskeleton. *J Biomech.* **2010**, *43*, 9-20.

(46) Al-Ani, A. W.; Zhang, L.; Ferreira, L.; Turyanska, L.; Bradshaw, T. D.; Thomas, N. R Listeria innocua Dps as a nanoplatform for bioluminescence based photodynamic therapy utilizing Gaussia princeps luciferase and zinc protoporphyrin IX. *Nanomedicine (N.Y., NY, U.S.)* **2019**, *20*, 102005.

(47) Wick, W.; Platten, M.; Weller, M. New (alternative) temozolomide regimens for the treatment of glioma. *Neuro-oncology* **2009**, 11(1), 69-79.

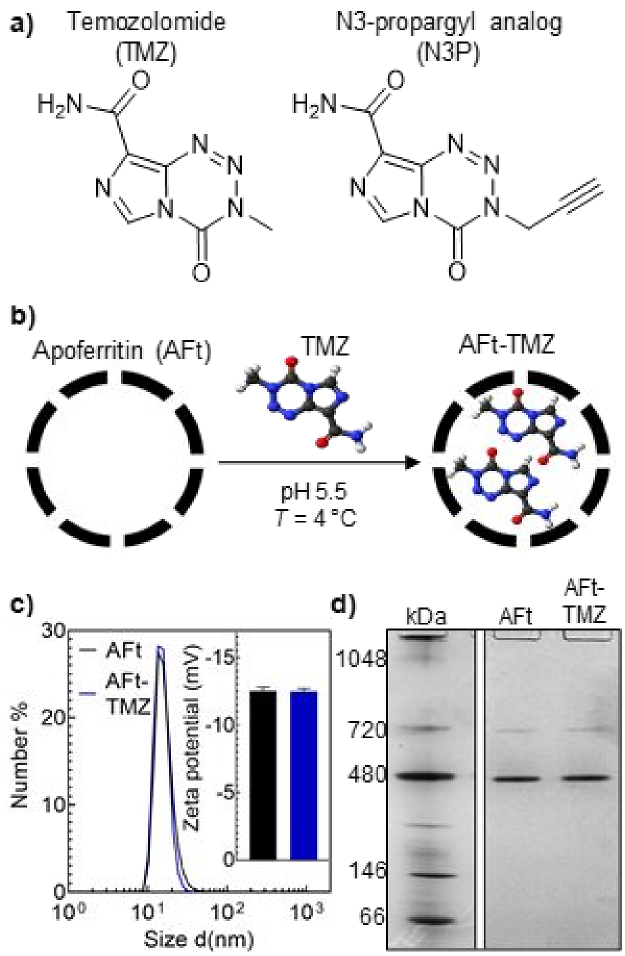

Figure 1. **(a)** Chemical structures of TMZ and N3P. **(b)** Illustration of the encapsulation of TMZ into AFt by the nanoreactor route. **(c)** Hydrodynamic size distribution of AFt and AFt-TMZ measured by dynamic light scattering and (Inset) corresponding zeta potential values. (**d)** Native-PAGE of AFt and AFt-TMZ performed on a 4-16% gradient gel.

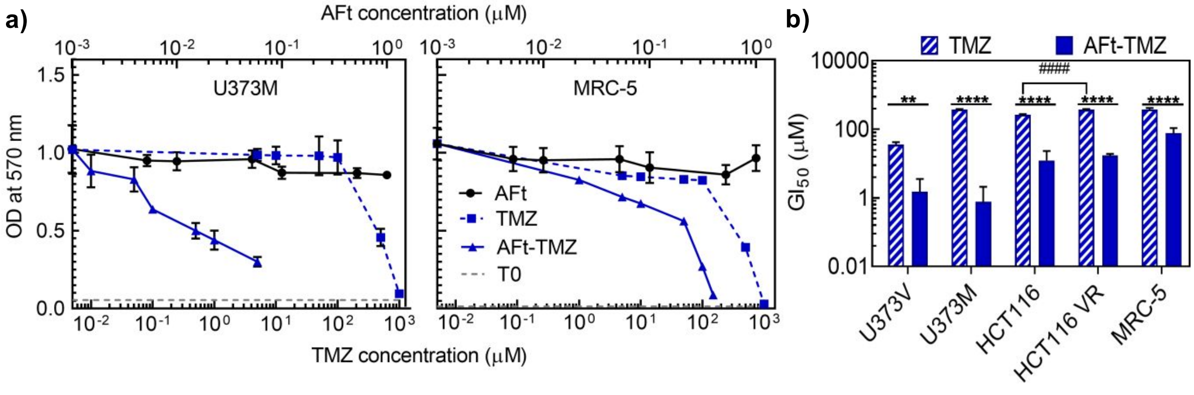

Figure 2. (a) *In vitro* cytotoxicity profiles for U373M (GBM cells, MGMT +) and non-cancerous MRC 5 fibroblasts following 6-day exposure to AFt, TMZ and AFt-TMZ. (**b)** A summary of GI_{50} values for TMZ and AFt-TMZ in all studies cell lines. Values are reported as mean ± SD (n > 3). $^{**}P < 0.01$ and $^{****}P < 0.0001$.

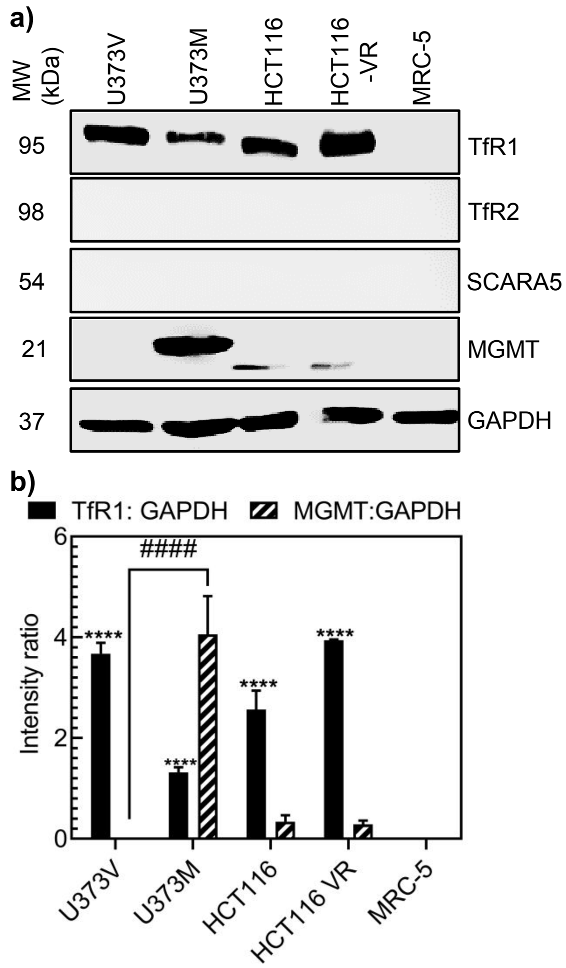

Figure 3. Cellular characterization of protein expression. **(a)** Western blot analysis of membrane bound receptors responsible for AFt uptake and intracellular proteins responsible for TMZ resistance. **(b)** Quantification of target protein band intensity expressed as a ratio of target protein to loading control (GAPDH) band intensity using the LICOR software. Values are reported as mean ± SD (n = 3). Significant difference from MRC-5 are expressed as ****P < 0.0001; Significant difference from U373V is expressed as $^{####}P < 0.0001$.

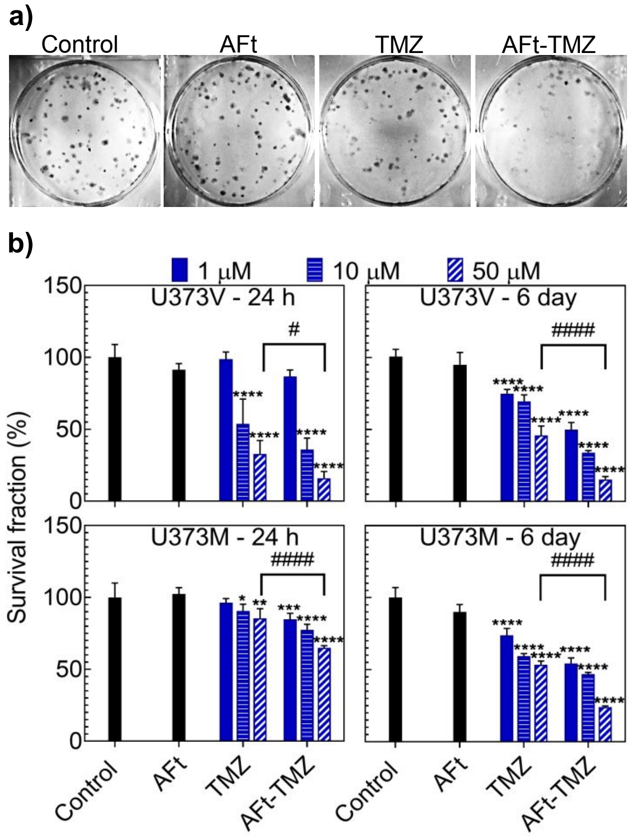

Figure 4. *In vitro* characterization of cell proliferation proficiency following treatment. **(a)** Representative images of the clonogenic assay conducted on U373M for a 6-day treatment (TMZ 50 µM, AFt-TMZ 50 µM, AFt 0.057 µM or media alone) exposure. **(b)** Percentage survival fraction of GBM; MGMT +/- cells following either a 24 h or 6-day treatment regimen with 1, 10 or 50 µM TMZ/ AFt-TMZ and 0.057 µM AFt (equivalent to AFt concentration of AFt-TMZ 50 µM). Values are reported as mean ± SD (n = 5). Significant difference from the control are expressed as $^{*}P < 0.05$, $^{**}P < 0.01$, $^{***}P < 0.001$ and $^{****}P < 0.0001$. Significant difference from TMZ are expressed as $^{\#}P < 0.05$. $^{\#\#\#\#}P < 0.0001$.

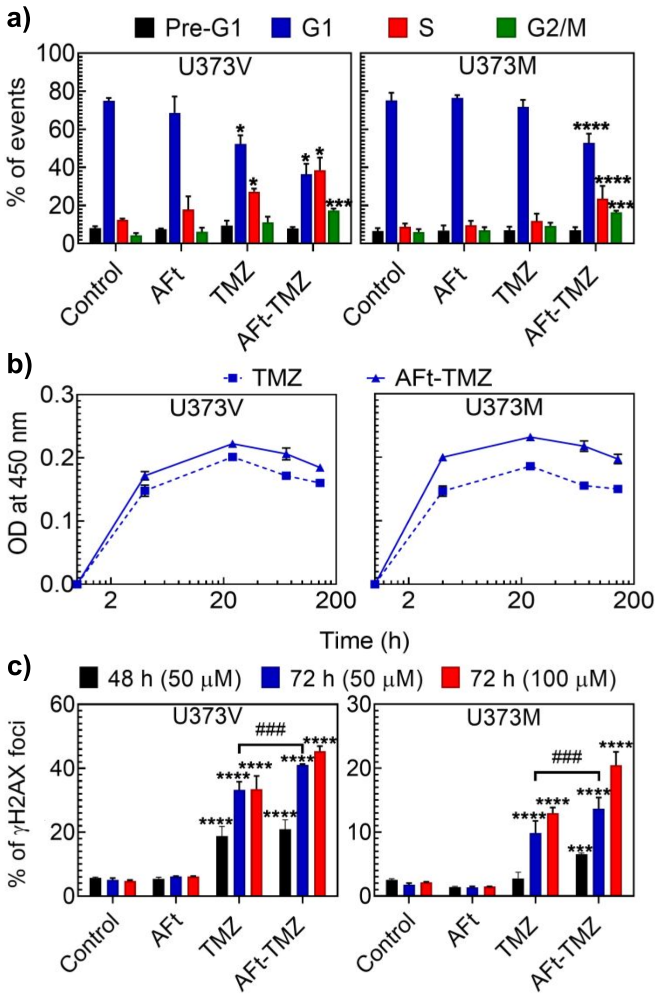

Figure 5. The mechanism of action of TMZ versus AFt delivered TMZ in GBM, MGMT +/- cells. **(a)** Summary of the number of gated events i.e. cells (expressed as a percentage from 10000 gated events), arrested in different phases of the cell cycle after 72 h treatment (TMZ 50 μM, AFt-TMZ 50 μM, AFt 0.057 μM or media alone) exposure. **(b)** ELISA DNA *O6*-MeG quantification following exposure of cells to 50 μM of TMZ or AFt-TMZ. **(c)** Summary of the fluorescence intensity of γH2AX foci (expressed as a percentage from 10000 gated events), after a 48 or 72 h treatment exposure to 50 or 100 μM of TMZ and AFt-TMZ and 0.057 or 0.1 μM of AFt. Values are reported as mean ± SD (n = 3). Significant difference from the control are expressed as **P* < 0.05, ****P* < 0.001 and *****P* < 0.0001. Significant difference from TMZ are expressed as ###*P* < 0.001.

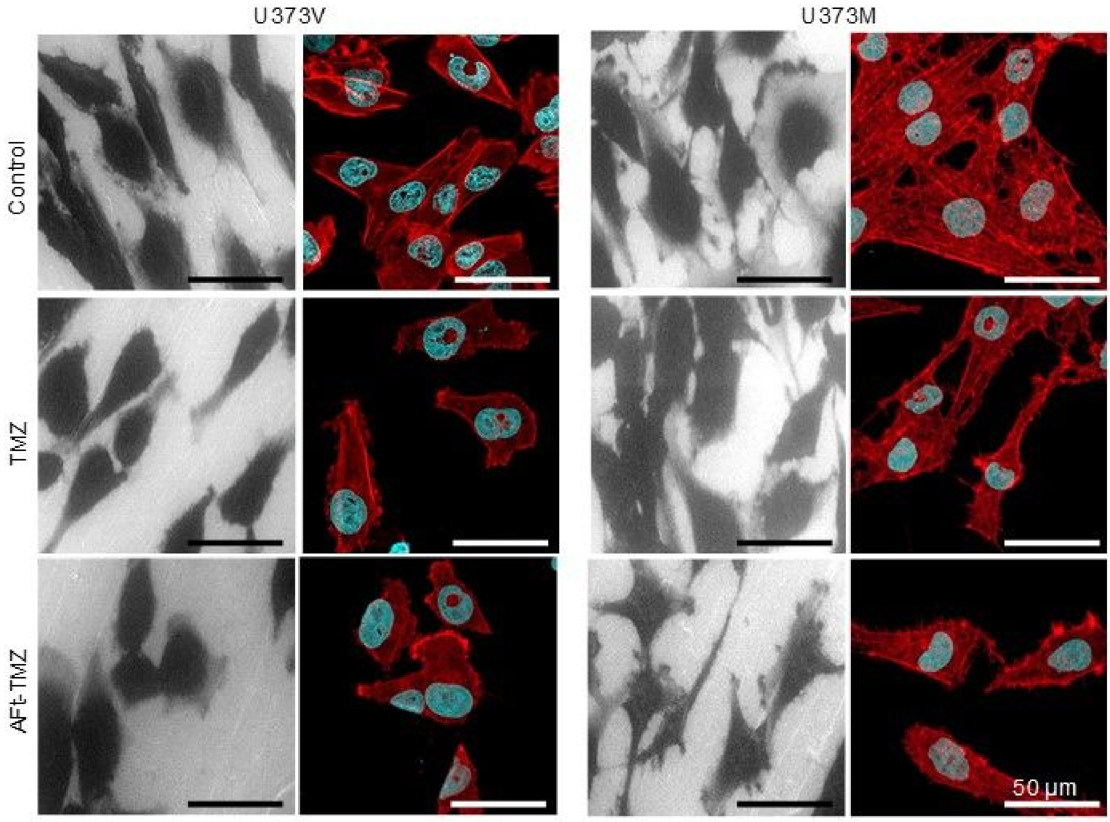

Figure 6. Morphological changes to GBM cells following 24 h treatment exposure (TMZ/ AFt-TMZ 50 μM). Cell surface morphology was monitored by a combination of ESEM and confocal microscopy (phalloidin (red) - F-actin staining; DAPI (blue) – nucleus staining). Scale bar is 50 μm.

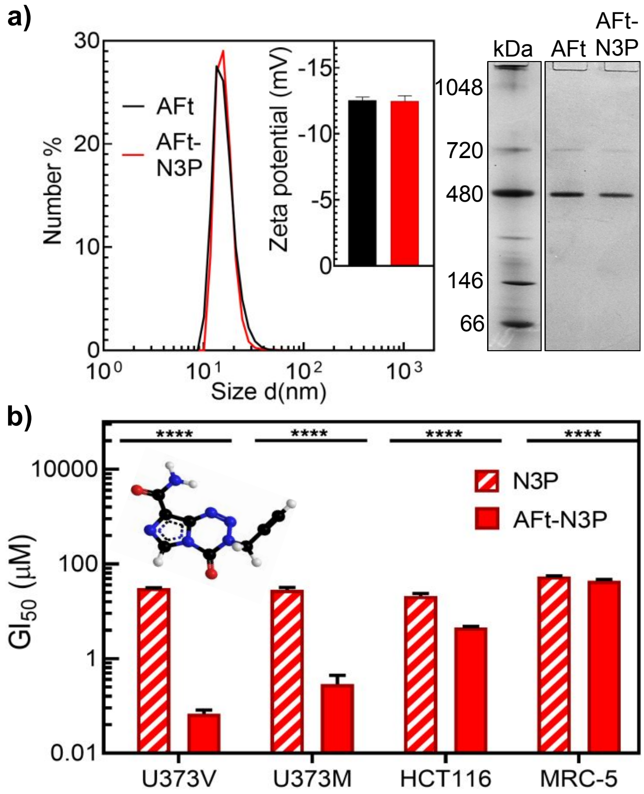

Figure 7. (a) Hydrodynamic size distribution of AFt and AFt-N3P measured by dynamic light scattering and (inset) corresponding zeta potential measurements. In addition, native-PAGE carried out on AFt and AFt-N3P showing protein integrity was performed on a 4-16% gradient gel. **(b)** *In vitro* cytotoxicity MTT studies with naked and encapsulated N3P (TMZ analog; inset chemical structure shown). Summary of concentration values leading to growth inhibition at 50% (GI_{50}) for test agents against GBM (MGMT +/-), HCT116 (MMR -) and non-cancerous MRC-5 cells. Values are reported as mean ± SD (n=5). ****P < 0.0001.

TABLE OF CONTENTS graphics